# Hydrodynamics and absorption efficiencies of wavemakers

A.E. Maguire[1] and D.M. Ingram[2]

[1]Institute for Energy Systems,
Joint Research Institute for Energy ,
The University of Edinburgh,
E-mail: E.Maguire@ed.ac.uk
[2] E-mail: David.Ingram@ed.ac.uk

## Abstract

For most of the twentieth century naval hydrodynamics, and more recently, wave energy hydrodynamics have been limited to the realms of theory and physical experiments. Both of these methods of fluid flow analysis are constrained through scope, cost and size of facility. The advent of high speed digital computing has brought with it a new dimension for analysing fluid flows, that of numerical modelling. This paper aims to harness this progress in computing power and established commercial computational fluid dynamics (CFD) codes to create a numerical analogue to the physical test flumes that are in operation in many hydrodynamic labs. Using numerical wavemakers will allow for the use of different shaped wavemakers that would be otherwise impossible to implement in a physical waveflume, these non-conventional shapes will be investigated.

This paper presents the well established wavemaker theory. This is then adapted to obtain the hydrodynamic coefficients of added mass and damping for two novel shaped wavemakers. The different wavemaker geometries are compared on the basis of their theoretical wave absorption efficiencies at various tuned frequencies. Wavemaking simulations using ANSYS CFX are then presented and the results are discussed.

**Keywords:** Wavemaker, CFD, absorption, added mass, damping.

## 1 Introduction

A general theory for the generation of waves by oscillating solid boundaries was first prestented by Havelock [1] and is widely considered as the foundation of wavemaker theory. Building upon this knowledge, *Les Appareils Générateurs de Houle en Laboratoire* published by Biésel and Suquet [2] (later to be translated into English [3]) was a huge advancement in laboratory generated waves. It solved the analytical problem for a number of different wavemakers and geometries providing a transfer function relating the wave paddle displacement to the propagating wave amplitude. This linear transfer function has been confirmed through theoretical and experimental comparison [4],[5]. Building on these transfer functions Gilbert *et al.*[6] presented analysis of dimensionless values for the forces and paddle strokes which was used in the construction of the first wave tank at the University of Edinburgh.

A major problem encountered with wave tanks is that of wave re-reflections spoiling the test domain. Passive wave absorbers dealt with impinging waves adequately but problems with re-reflections from the wave makers and test devices persisted. In an attempt to show that it is possible to move a paddle in a manner that absorbs incident waves, Milgram [7] published his paper on “Active water-wave absorbers”. Milgram concluded that in the synthesis of a wave-absorbing system four criteria must be met: The complete system must be stable. Drift of the paddle must be prevented by the absorbing system and have zero response at a frequency of zero. To prevent high frequency noise, the absorbing system subfunction should be less than the hydrodynamic system function. And obviously, the reflection coefficient should be less than one for all frequencies. Milgram used surface elevation for the active feedback mechanism. He suggests that the exerted force acting on the paddle would be attractive to operate on but points to physical constraints in his specific flume. There was a short fluid filled space behind the wave paddle. The fluid motion in this small space would complicate calculations through resonance at certain frequencies, thus he concluded that it was not practical to activate the paddle on the basis of measured force. The surface elevation a short distance from the wave paddle was used instead. Milgram conducted experimental work to compare the measured and predicted wave reflection coefficients. Absolute reflection coefficients in the range of 2 % to 11 % were reported for frequencies between 1 to 4 Hz. It should be noted that this active absorber was not used in a combined generation and absorption mode.

Unaware of Milgrams work on wave absorption, Salter [8] proceeded to obtain an active wave maker using force measurement. Salter cited three advantages to this method. Force is an integral quantity measured over the entire wave maker front and using this measurement minimises any slight errors encountered with single point measurements. Force sensors can be entirely free from the chemical and biological vagaries of tank water. Most types of tank probes use either resistive gauges or capacitance gauges. Both of these are susceptible to corrosion, biological growths, oil and dust residues, all of which require frequent re-calibration which is unacceptable for a large array of wave makers. Finally, Salter cites the conservation of energy as another reason to choose force feedback. He states that the advantage of using a force measurement is its ease in combing it with a velocity measurement and therefore fixing the rate of energy given to the water. He argues that it is "better to provide the right amount of energy at each frequency than to try to enforce a sinusoidal form that the waves do not like". Thus controlling energy bypasses many of the non-linearity problems that arise when generating steep waves.

In numerical wave tanks, many methods exist to try and cope with reflected waves using purely mathematical methods. The periodic boundary condition is where the solution is assumed to be periodic in space, so that the values of the unknowns on one vertical boundary can be to equal those on the other vertical boundary of the domain. Another technique used to simulate infinite outer fields at finite distance is that of artificial damping also referred to as sponge layers. This is the process of applying a dissipative term to the equations near the boundary of the truncated domain. This dissipative term can be added to the free surface boundary condition as well as both the dynamic and kinematic boundary conditions. A novel approach was adopted by Orlanski [9] where he imposed Sommerfeld's condition on the boundary. The main advantage of this approach was that no information on the frequency of the approaching waves was needed. The Sommerfeld-Orlanske is probably the most widely used technique for numerical absorption of waves [10]. As this research hopes to create an numerical analogue to physical paddles, the method for dealing with wave re-reflections will be using a physically realisable method, namely that of force-feedback. For a more in depth discussion on numerical absorption boundary conditions, please consult Romante [10] for a detailed review.

Research from the *Laboratoire de Mécanique de Fluide* at *École Centrale de Nantes* has been published regarding a realisable control strategy for active absorbing wave makers. Maisondieu and Clement [11] were the first to publish their results on a force feedback-feedforward control loop for a piston wave absorber. They considered the problem of absorption of water waves by the horizontal motions of a vertical plane in responce to the hydrodynamic forces it experiences. They are quick to point out that a solution to this in the frequency domain is relatively easy, but upon implementation of an inverse Fourier transform the solution becomes a non-causal impulse response function. In their paper they propose to model the ideal controller by a causal approximation. They compare their new control strategy for two conditions, when one knows the dominant frequency in the incident waves and when one does not.

This publication was quickly followed up with another publication [12] on the same matter, conducting a comparison of time domain control laws for this piston wave absorber. Again this paper concentrated on the derivation of efficient time domain control strategies for the absorption of waves by a vertical paddle. This paper suggests two causal non-ideal approximations of the ideal non-causal controller. This method proved very promising at low frequencies, when one can identify a dominant frequency in the incident wave train *a priori*

Building on this published work Chatry and Clement [13] proposed a self-adaptive control of a piston wave absorber. This paper derived sub-optimal approximations similar to Maisondieu and Clement [11] but as the previous study showed better performance when the incident wave frequency was known, a self-adaptive tuner was developed hoping to maintain the system frequency to the optimal one. It is based on a frequency tracking extended Kalman filter algorithm and a feedforward loop. The efficiency of the controllers was measured by numerical experiments. It was found that this self-adaptive feedforward feedback system performed very well over a broad frequency range.

Newman [14] produced analysis of wave generation and absorption within the framework of linear potential theory. He derives relations that govern the control of the absorbers in an attempt to eliminate reflected waves from the walls of the basin. He sets out the theory behind control of wavemaking and absorbing in two-dimensions and progresses to extend this to the three-dimensional case. This paper encompasses the theoretical framework and analysis of the obtained results. It deals with conditions for optimisation of two-dimensional wavemakers in two and three dimensions. It then investigates the effects of including a floating body in the computational domain. Later in the paper two-dimensional wavemakers are analysed in the time domain.

In a recent paper, Spinneken and Swan [15] discuss causal approaches for controlling active wavemakers. Their technique is based upon infinite impulse response filters and they show that optimisation of this controller results in very good levels of absorption. They compare their results to the techniques of Naito [16] and ECN showing better performance with their control strategy.

## 2 Hydrodynamic coefficients of a wavemaker in a channel

Following the method used by Falnes [17, sect 5.2.3], let us consider a physical model shown in figure (1). Cartesian coordinates, $x, y, z$, are used, with $z = 0$ on the still water level and the $+ve\ z axis$ directed upwards. This is a 2D piston, in a water depth, $h$, that can oscillate in surge. When any body oscillates in water a radiated wave with a velocity potential, $\phi_r$ is generated. This will be a linear combination of the six modes of oscillation giving

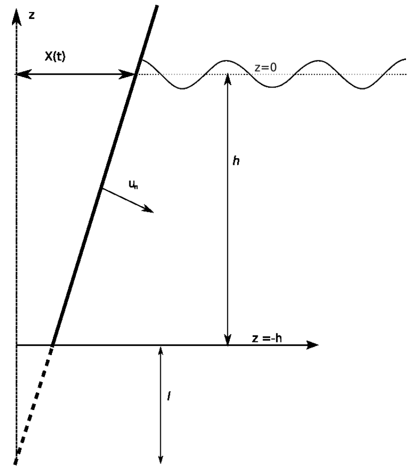


**Figure 1:** Two-Dimensional Wave Flume Definition Sketch

[17];

$$\hat{\phi}_r = \sum_{j=1}^{6} \varphi_j \hat{u}_j \tag{1}$$

where $\varphi_j$ is a complex coefficient of proportionality. In the case shown, the piston motion is limited to surge ($j = 1$). If the piston has a complex velocity with complex amplitude $\hat{u}_1 \neq 0$, then according to the inhomogeneous boundary condition

$$\frac{\partial \varphi_1}{\partial x} = c(z) \qquad for x = 0 \tag{2}$$

where $c(z)$ is a function that defines the shape profile of the wavemaker. The general form of $c(z)$ for a two-dimensional wavemaker is

$$c(z) = \left(1 + \frac{z}{h+l}\right) \tag{3}$$

where $l$ is the hinge depth. As $l \to \infty$, c(z) corresponds to the surface profile of a piston ($c(z) = 1$) or as $l \to 0$ the profile is that of a bottom hinged paddle ($c(z) = 1 + \frac{z}{h}$) Following Havelock [1] and Falnes [17] , $\varphi_1$ can be represented as

$$\varphi_1 = c_0 Z_0(z) e^{-ik_0 x} + \sum_{n=1}^{\infty} c_n Z_n(z) e^{-k_n x} = \sum_{n=0}^{\infty} X_n(x) Z_n(z) \tag{4}$$

where

$$X_n(x) = c_n e^{k_n x} \tag{5}$$

Here, $k_n$ is the solution to the dispersion relationship for $n \geq 1$ and conveniently letting $k_0 = ik$ [17]

$$\omega^2 = -gik_n \tanh(-ik_n h) \tag{6}$$

Making use of the boundary condition (eqn. 2) gives

$$c(z) = \left[\frac{\partial \varphi_1}{\partial x}\right] = \sum_{n=0}^{\infty} X_n'(0) Z_n(z) \tag{7}$$

As Falnes [17] shows, multiplying by the complex conjugate, $Z_m^*(z)$ and integrating from $z = -h$ to $z = 0$ while using orthogonality condition gives

$$\int_{-h}^{0} c(z) Z_m^*(z) dz = \sum_{n=0}^{\infty} X_n'(0) \int_{-h}^{0} Z_m^*(z) Z_n(z) dz = X_m'(0) h \tag{8}$$

That is,

$$X_n'(0) = \frac{1}{h} \int_{-h}^{0} c(z) Z_n^*(z) dz \tag{9}$$

Combining equation (9) and equation (5) yields

$$X_0'(0) = ik_0 c_0, \qquad X_n'(0) = k_n c_n \tag{10}$$

Thus giving the two coefficients

$$c_0 = \frac{-1}{ik_0 h} \int_{-h}^{0} c(z) Z_0^* dz \tag{11}$$

$$c_n = \frac{-1}{k_n h} \int_{-h}^{0} c(z) Z_n^* dz \tag{12}$$

The orthogonal set of eigenfunctions $Z_n(z)$ are given as [see 17, chap. 4.2]

$$Z_0 = (N_0)^{-1/2} \cosh(k_0(z+h)) \tag{13}$$

$$Z_n = (N_n)^{-1/2} \cos(k_n(z+h)) \tag{14}$$

where

$$N_0 = \frac{1}{2}\left(1 + \frac{\sinh(2k_0 h)}{2k_0 h}\right) \tag{15}$$

$$N_n = \frac{1}{2}\left(1 + \frac{\sin(2k_n h)}{2k_n h}\right) \tag{16}$$

The radiation impedance of the wavemaker in a two-dimensional channel acting in surge is given by Falnes [17]. The term $R_{j'j}$ is the radiation resistance matrix or added damping. $X_{j'j}$ is the radiation reactcance matrix and $m_{j'j}$ is the added mass.

$$\begin{aligned} Z_{j'j} &= R_{j'j} + iX_{j'j} \\ &= R_{j'j} + i\omega m_{j'j} \\ Z_{11} &= i\omega\rho d \int_{-h}^{0} \left[\psi_1 \frac{\partial \varphi_1^*}{\partial x} dz\right]_{x=0} dz \end{aligned} \tag{17}$$

Thus, the impedance per unit width

$$\begin{aligned} \frac{Z_{11}}{d} &= i\omega\rho \int_{-h}^{0} \left[c_0 Z_0(z) + \sum_{n=1}^{\infty} c_n Z_n(z)\right] c^*(z) dz \\ Z_{11}' &= i\omega\rho \left[c_0(-ik_0 h) c_0^* + \sum_{n=1}^{\infty} c_n (k_n h) c_n^*\right] \\ &= \omega k_0 \rho h |c_0|^2 + i\omega\rho h \sum_{n=1}^{\infty} k_n |c_n|^2 \end{aligned} \tag{18}$$

The radiation resistance, $R_{11}$, or added damping is the real part of eq.18

$$R_{11} = \Re\{Z_{11}\} = \omega k_0 \rho h d |c_0|^2 \tag{19}$$

and the added mass, $m_{11}$, is the imaginary part of eq.18

$$m_{11} = \Im\{Z_{11}\} = \rho h d \sum_{n=1}^{\infty} k_n |c_n|^2 \tag{20}$$

### 2.1 Derivation of added mass and damping for a bottom hinged paddle

As can be seen, both the added mass and damping are functions of $c_0$ and $c_n$ respectively. These parameters are in turn functions of the shape parameter, $c(z)$. Thus for different paddle shapes, the added mass and added damping will vary significantly. The two main shapes of concern, in a physical wavemaker, are that of a piston ($c(z) = 1$) and a bottom hinged flap ($c(z) = 1 + z/h$). The following equations are a derivation of the added mass and damping for the latter, a bottom hinged flap. This derivation was not presented by Falnes [17], but the added mass and damping coefficients agree with those presented by Newman [14] for a bottom hinged flap.

From equation (11) and using equation (13)

$$\begin{aligned} c_0 &= -\frac{1}{ik_0h}N_0^{-1/2}\int_{-h}^{0}(1+z/h)\cosh(k_0(z+h))dz \\ &= -\frac{1}{ik_0h}N_0^{-1/2}\frac{1+k_0h\sinh(k_0h)-\cosh(k_0h)}{{k_0}^2h} \\ &= i\left(1+k_0h\sinh(k_0h)-\cosh(k_0h)\right){k_0}^{-3}h^{-2} \\ &\left(\frac{1}{2}+\frac{1}{4}\frac{\sinh(2k_0h)}{k_0h}\right)^{-1/2} \end{aligned} \tag{21}$$

$$\begin{aligned} R_{11} &= \omega k_0\rho hd|c_0|^2 \\ &= 4\,\frac{\omega\rho\,\left(1+\sinh(k_0h)k_0h-\cosh(k_0h)\right)^2}{{k_0}^4h^2\left(2k_0h+\sinh(2k_0h)\right)} \end{aligned} \tag{22}$$

Similarly, from equation (12) and using equation (14)

$$\begin{aligned} c_n &= -\frac{1}{k_nh}N_n^{-1/2}\int_{-h}^{0}(1+z/h)\cos(k_n(z+h))dz \\ &= \frac{1}{k_nh}N_n^{-1/2}\frac{-1+\cos(k_nh)+k_nh\sin(k_nh)}{{k_n}^2h} \\ &= \left(-1+\cos(k_nh)+k_nh\sin(k_nh)\right){k_n}^{-3}h^{-2} \\ &\left(\frac{1}{2}+\frac{1}{4}\frac{\sinh(2k_n)}{k_n}\right)^{-1/2} \end{aligned} \tag{23}$$

$$\begin{aligned} m_{11} &= \omega\rho hd\sum_{n=1}^{\infty}k_n|c_n|^2 \\ &= 4\rho\sum_{n=1}^{\infty}\frac{\left(-1+\cos(k_nh)+\sin(k_nh)k_nh\right)^2}{{k_n}^4h^2\left(2k_nh+\sin(2k_nh)\right)} \end{aligned} \tag{24}$$

### 2.2 Added mass and damping coefficients for different paddle geometries

As shown in section 2.1 the added mass and damping are dependant on the wavemakers geometry. The following results show the added mass ($m_{11}$) and damping ($R_{11}$) for four different geometries. The standard piston and bottom hinged geometries that are widely used in many hydrodynamic laboratories around the world. Also included are coefficients for a hyperbolic paddle which matches the boundary condition of the wave velocity profile. This results in a wave maker with no evanescent modes, thus no local waves, at one particular wave frequency. The other is the unique case of a wavemaker with no progressive waves, just a local standing wave. These situations of no progressive waves and no evanescent waves are difficult to achieve in a physical wave flume but could be more easily achieved in a numerical model.

#### 2.2.1 Piston Wavemaker

The unit displacement of a two-dimensional piston-type wave maker is $c(z) = 1$. Under oscillations corresponding to equation (1) this results in the entire boundary moving in unison, as would be expected. Following a the derivation outlined in section 2.1 the following added mass and damping were obtained in a similar manner.

$$m_{11} = 4\sum_{n=1}^{\infty}\frac{\rho\left(1-\left(\cos(k_nh)\right)^2\right)}{{k_n}^2\left(2k_nh+\sin(2k_nh)\right)} \tag{25}$$

$$R_{11} = 4\,\frac{\omega\rho\left(\left(\cosh(k_0h)\right)^2-1\right)}{{k_0}^2\left(2k_0h+\sinh(2k_0h)\right)} \tag{26}$$

#### 2.2.2 No local waves

For there to be no local or evanescent waves, there should be no added mass. This can be achieved if the paddle velocity matches that of the wave field. This is done by setting the unit displacement to

$$c(z) = \frac{\cosh(k_p(z+h))}{\cosh(k_ph)} \tag{27}$$

It should be noted that the wave number, $k_p$, is frequency dependant and therefore this wavemaker will have no added mass at only one chosen frequency - the frequency corresponding to the respective wavenumber value, $k_p = k(\omega_p)$. The resulting added mass and damping are

$$\begin{aligned} m_{11} = \sum_{n=1}^{\infty}\rho\,e^{-c}\Bigg(&\frac{(k_pe^c-k_pe^{b+c}-k_pe^b+k_p}{\left(2k_nh-i\sinh(c)\right)\left(e^b+1\right)^2} \\ &\frac{-ik_n+ik_ne^{b+c}-ie^bk_n+ik_ne^c)^2}{\left({k_p}^2+{k_n}^2\right)^2}\Bigg) \end{aligned} \tag{28}$$

$$\begin{aligned} R_{11} = \omega\rho\Bigg(&\frac{(k_0e^{-i(b+ia)}-k_0+e^ak_0-k_0e^{-ib}}{4\left(a+\sinh(a)\right)\left(\cos(b/2)\right)^2} \\ &\frac{-e^{-ib}k_p+k_p+e^ak_p-k_pe^{-i(b+ia)})^2}{\left({k_p}^2-{k_0}^2\right)^2}\Bigg)e^{i(b+ia)} \end{aligned} \tag{29}$$

where the substitution of $a = 2k_0h$, $b = 2ik_ph$ and $c = 2ik_nh$ have been. As mentioned, for there to be no evanescent waves, the added mass should be zero (at that specific frequency defining the shape $k_p(\omega)$ for $\omega = \pi, 2\pi, 3\pi$, which is the case (figs. 2a,2b,2c)

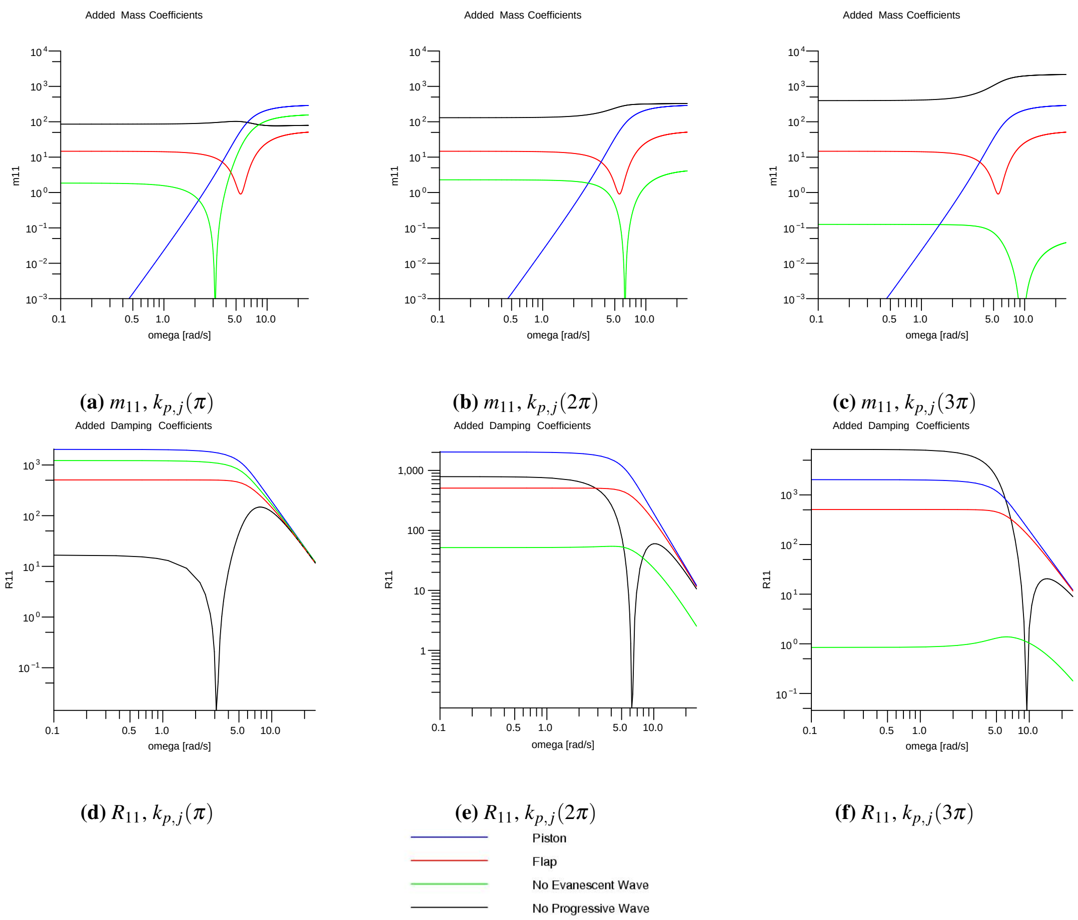


**(a)** $m_{11}, k_{p,j}(\pi)$ **(b)** $m_{11}, k_{p,j}(2\pi)$ **(c)** $m_{11}, k_{p,j}(3\pi)$

**(d)** $R_{11}, k_{p,j}(\pi)$ **(e)** $R_{11}, k_{p,j}(2\pi)$ **(f)** $R_{11}, k_{p,j}(3\pi)$

**Figure 2:** Hydrodynamic coefficients, added mass, top and damping, bottom, for piston, bottom hinged flap, no evanescent waves and no progressive wave wavemakers. The no evanescent and no progressive wavemakers are for three different geometries based on wave numbers $k(\omega_{p,j})$ for $\omega_{p,j} = \pi, 2\pi, 3\pi$

#### 2.2.3 No progressive waves

This is another special case were the paddle will move in such a way that only an evanescent wave will be present. This would be very difficult to achieve in a physical wave maker, but could be more easily achieved in a numerical code. For this to occur, the wavemaker needs to move according to the following $c(z)$ in the case of $n = j$ where $j$ is a single solution to equation (6)

$$c(z) = \frac{\cos(k_j(z+k))}{\cos(k_jh)} \tag{30}$$

Again, the the geometry is dependant on the selection of a wave number at a particular frequency, $k_j = k_j(\omega_j)$. This choice of $c(z)$ results in the upper and lower parts of the vertical wall oscillating out of phase with each other. The number of oscillations between the bottom of the tank and still water lever (SWL) depends on the choice of $j$. The resulting added mass and damping are given as

$$m_{11} = 4\rho \frac{(-k_j\sin(k_jh)\cos(k_nh) + k_n\cos(k_jh)\sin(k_nh))^2}{(2k_nh+\sin(2k_nh))(\cos(k_jh))^2 \left(-k_j^2+k_n^2\right)^2} \tag{31}$$

$$R_{11} = \omega\rho \left( \frac{(-k_0e^{a+b}+k_0e^b-k_0e^a+k_0-ik_j + ik_je^b-ik_je^a+ik_je^{a+b})^2 e^{-a-b}}{4(a+\sinh(a))\left(\cosh\left(\frac{b}{2}\right)\right)^2 \left(k_0^2+k_j^2\right)^2} \right) \tag{32}$$

where the substitution of $a = 2k_0h$ and $b = 2ik_jh$ have been made.

For the three different geometries based upon choice of $k_j(\omega)$ for $\omega = \pi, 2\pi, 3\pi$ it can be seen (figs. 2d,2e,2f) that the damping is zero at these frequencies. For all of these solutions, $j = 1$ resulting in just one oscillation between the tank bottom and SWL increasing the value of $j$ will, in turn, increase the number of oscillations between the SWL and the bottom of the flume.

The non-dimensionalised added mass and damping coefficients for all four shapes are shown in figure (2).

## 3 Basic Theory of Wave Absorption

### 3.1 Absorption efficiency

A concept used by Naito [16] and presented further by Spinneken [15] is that of absorption efficiency. Naito [16] presented an absorption coefficient, $C_e(\omega)$ measuring the power absorbed by the external mechanism. The condition of causality was discussed and a power absorption with fixed coefficients $C_{ec}$ was also presented. This resulted in less than all of the available power being absorbed in irregular waves as the system was only optimised for one frequency.

According to Falnes [17] the intrinsic impedance, $Z_i$ can be represented as

$$Z_i(\omega) = R(\omega) + i\left(\omega\left[M + m(\omega)\right] - \frac{c}{\omega}\right) \quad (33)$$

Where $M$ is the mass of the paddle, $c$ is the spring stiffness, $m(\omega)$ and $R(\omega)$ are added mass and damping, respectively, and where the subscripts for surge have been omitted

Following the same author and many others, the optimum control force occurs when the control impdance, $Z_u$ equals the complex conjugate of the intrinsic impedance

$$Z_u(\omega) = Z_i^*(\omega) = Z_{u,OPT}(\omega) \quad (34)$$

Thus,

$$Z_{u,OPT}(\omega) = R(\omega) - i\left(\omega\left[M + m(\omega)\right] - \frac{c}{\omega}\right) \quad (35)$$

and under a fixed coefficient system tuned to $\omega = \omega_p$,

$$Z_{u,OPT}(\omega_p) = R(\omega_p) - \left(i\left[\omega_p\left(M + m(\omega_p)\right) - \frac{c}{\omega_p}\right]\right) \quad (36)$$

$$= R_p - \left(i\left[\omega_p\left(M + m_p\right) - \frac{c}{\omega_p}\right]\right) \quad (37)$$

where $R_p$ and $m_p$ denotes fixed coefficients at $\omega = \omega_p$

Under a two coefficient ($r_u$ and $c_u$) control system, the control force in the time domain is represented as

$$f_u(t) = r_u u(t) + c_u x(t) \quad (38)$$

and thus the impedance in the frequency domain is

$$Z_u(\omega) = r_u + \frac{c_u}{i\omega} \quad (39)$$

and optimising equation (39) at a single frequency, $\omega_p$, results in

$$Z_u(\omega_p) = r_u - \frac{ic_u}{\omega_p} \quad (40)$$

Price [18] compared equations (36) and (40) showing control coefficients of

$$r_u = R_p \quad (41)$$

$$c_u = \left(\omega_p^2(M + m_p) - c\right) \quad (42)$$

replacing back into equation (39), [18] presented the tuned control impedance at $\omega_p$, with two control settings, over the full range of frequencies as

$$Z_u(\omega) = R_p - \frac{i}{\omega}\left[\omega_p^2\left(M + m_p\right) - c\right] \quad (43)$$

Falnes [17] shows that the absorbed useful power is given as

$$P_u = \frac{1}{2}\Re\left[Z_u(\omega)\right]\frac{|\hat{F_{e,j}}|^2}{|Z_i(\omega) + Z_u(\omega)|^2} = \frac{R_u(\omega)|\hat{F_{e,j}}|^2/2}{\left[R_i(\omega) + R_u(\omega)\right]^2 + \left[X_i(\omega) + X_u(\omega)\right]^2} \quad (44)$$

Setting the control impedance, $Z_u(\omega)$ to the complex conjugate of the intrinsic impedance $Z_i^*$, namely setting the variables $R_u(\omega)$ and $X_u(\omega)$ to their optimum values of $R_i(\omega)$ and $-X_i(\omega)$ gives an expression for the maximum power

$$P_{u,max} = \frac{|\hat{F}_{e,j}|^2}{8R_i} \quad (45)$$

Combining these equations (eqns 44,45), the absorption coefficient, similar to that of Naito [16] and Spinneken [15], for a fixed coefficient system can be shown as

$$\frac{P_u}{P_{u,max}} = 4\frac{R_u(\omega)R_i(\omega)}{\left(R_i(\omega) + R_u(\omega)\right)^2 + \left(X_i(\omega) + X_u(\omega)\right)^2} \quad (46)$$

Using equations (33,36) the power absorption ratio can be represented as

$$\frac{4\omega^2 R_p R(\omega)}{\omega^2\left[R_p + R(\omega)\right]^2 + \left[(\omega^2 - \omega_p^2)M + \omega m(\omega) - \omega_p^2 m_p\right]^2} \quad (47)$$

### 3.2 Absorption for different wavemakers

Absorption ratios, $P_u/P_{u,max}$, for different wavemaker shapes (Piston, Bottom hinged Paddle, No Evanescent waves, No Progressive Waves) are shown in figure (3). These figures compare the fraction of waves that can be theoretically absorbed equation (46) by the four different wave makers with different choices of tuning frequency and shape frequency. For the piston and paddle shaped wavemakers, the only handle on control is by setting the tuning frequency $\omega_p$. For the other two types of wave maker - their shape parameter $c(z)$, is a function of wave number and thus frequency dependant. For these wavemakers a second control variable, $k_j$ and $k_p$ is available. Both of these control handles are varied from 0.5 Hz and 1.5 Hz. This range of frequencies is comparable to that of the tank used at Edinburgh University, and most tanks used in small scale hydrodynamic laboratories.

The absorption characteristics for piston and flap wavemakers only varies due to a change in tuning frequency, $\omega_p$. When the shape function is set to $k_{p,j}(\omega) = k_{p,j}(\pi)$ the bottom hinged paddle attains the highest absorption, followed by the hyperbolic paddle with $k_p = k(\pi)$ (eqn.27) and then piston wave maker. The reason for this is setting the shape parameter to $k_{p,j}(\omega) = k_{p,j}(\pi)$, results in a hyperbolic shape in between that of a piston and a flap, thus explaining why the absorption characteristics are in between that of the paddle and flap.

Outwith $k_p(\omega) = k_p(\pi)$ ,the hyperbolic shaped paddle, with no evanescent waves (eqn.27), has better absorption characteristics than all other paddles regardless of their tuning frequency. This is unsurprising as the hyperbolic profile matches that of the Airy's velocity potential more closely than that of the either the piston or the flap. The big difference is that the hyperbolic shaped paddle has two handles of control. That of the tuning frequency, $\omega_p$ similar to the flap and piston, but it also has

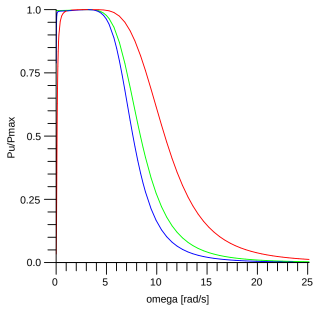


**(a)** $\omega_p = \pi;\, k_{pj}(\pi)$

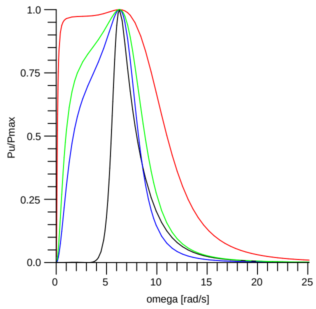


**(b)** $\omega_p = 2\pi;\, k_{pj}(\pi)$

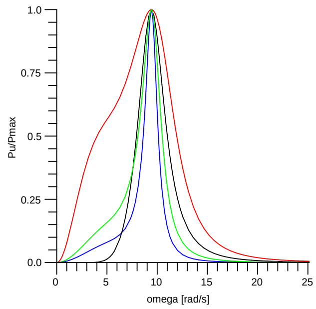


**(c)** $\omega_p = 3\pi;\, k_{pj}(\pi)$

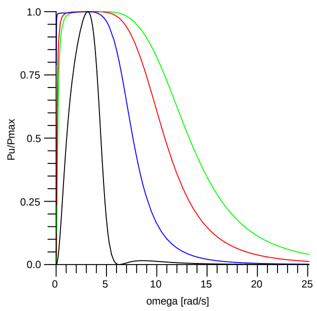


**(d)** $\omega_p = \pi;\, k_{pj}(2\pi)$

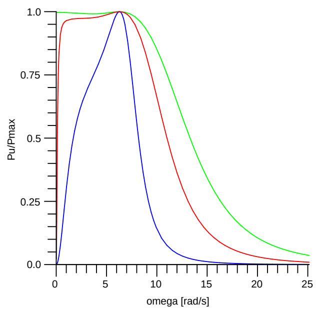


**(e)** $\omega_p = 2\pi;\, k_{pj}(2\pi)$

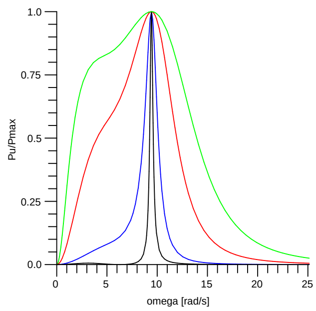


**(f)** $\omega_p = 3\pi;\, k_{pj}(2\pi)$

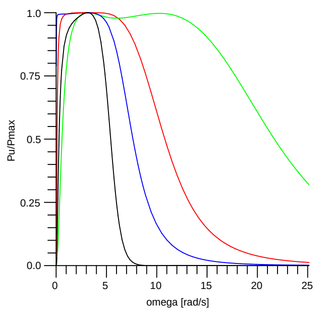


**(g)** $\omega_p = \pi;\, k_{pj}(3\pi)$

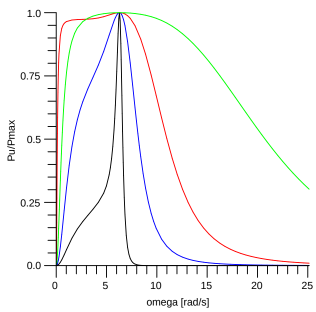


**(h)** $\omega_p = 2\pi;\, k_{pj}(3\pi)$

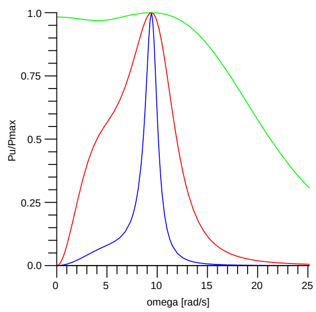


**(i)** $\omega_p = 3\pi;\, k_{pj}(3\pi)$

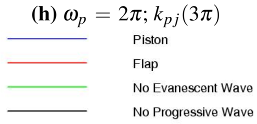


**Figure 3:** Graphs showing the absorption coefficients $\vartheta$ for different tuning frequencies, $\omega_p = \pi,\ 2\pi,\ 3\pi$ (columns) and different geometry shapes $k_{p,j}(\omega)$ for $\omega = \pi,\ 2\pi,\ 3\pi$ (rows)

a geometry control where the shape of the paddle can be designed to minimise the evanescent waves at one specific frequency, thus resulting in two sweet spots of control at $\omega_p$ and $k(\omega_p)$. Having these two handles of control, tuning frequency and shape can result in a far wider bandwith of absorption that would otherwise be achieved using either a regular piston or flap wave maker (fig.3).

One of the interesting results occurs for the case where the paddle is controlled in such a manner to have no progressive waves. As can be seen, this paddle can achieve some absorption when $k_j \neq \omega_p$. When the geometry shape, $k_j(\omega)$ is chosen such that $\omega = \omega_j$, as is the case in the diagonal of the 3*x*3 matrix in figure (3). Under these conditions the absorption of the *no progressive wave* paddle results in zero absorption. The reasons for this can be attributed to the old addage, *"a good wave absorber is a good wave maker "*. As this wavemaker cannot generate any progressive waves at this frequency, it cannot radiate waves to cause destructive interference, cancelling out the reflected waves thus there is zero wave absorption.

## 4 CFD simulation of wavemaker

This section describes the methods used to generate waves in a numerical wave tank using ANSYS CFX.

The dimensional values for the geometry of the numerical wave tank (NWT) were chosen such to be comparable to those in Edinburgh's long tank. The length of

Table 1: Dimensions of grids used

| | Coarse | Medium | Fine |
|---|---|---|---|
| No. elements Y1 | 10 | 20 | 40 |
| $\Delta Y$ [m] | 0.02 | 0.01 | 0.005 |
| No. elements Y2 | 20 | 40 | 40 |
| No. elements X | 390 | 780 | 1560 |
| $\Delta X$ [m] | 0.04 | 0.02 | 0.01 |
| No. Nodes | 38,318 | 157,762 | 377,762 |
| No. Elements | 18,720 | 78,000 | 187,200 |

the tank is $l = 15.6[m]$ with a water depth of $h = 0.8[m]$. The desired wave has a period of 1 $[s]$ and wave of amplitude 0.08 $[m]$. According to the wave dispersion relationship

$$\lambda = \frac{g}{2\pi}T^2 tanh\frac{2\pi h}{\lambda} \tag{48}$$

the wave length of such a wave is $\approx 1.56[m]$ with $d/\lambda = 0.514$ (deep water conditions). This results in the tank being ten wavelengths long. The phase speed, $c = \frac{\lambda}{T}$, of these waves is $1.56[m/s]$, and the group velocity $c_g = \frac{1}{2}c = 0.78[m/s]$.

Three different grids were used to compare the effects of refinement and to check for convergence, referred to as coarse, medium and fine. The cell dimensions for the initial coarse mesh were based upon the expected free surface elevation and on the phase speed of the wave. The remaining two meshs' dimensions were iterative refinements of the coarse mesh. As the main area of interest is the wave's free surface, extra mesh refinement is used in this region. This area of refinement extended from $\pm 0.1[m]$ around the SWL. The mesh distribution in this area was uniform, the areas above and below this region, extending to the NWT bottom and top opening, have a stretched geometric distribution along a distance of $0.7[m]$ (fig.4). Mesh dimensions for the three different meshes are as follows; For all grids, the domain is split into two regions, one with a distance of a single wavelength, $\lambda$ from the paddle. This region allows mesh motion. The other region, making up the rest of the mesh is stationary (fig.4). This is was chosen after advice and correspondence with CFX support. It was said that mesh motion, by its very nature is a diffusive process and will lead to unsatisfactory results. Mesh motion is needed in the region near the paddle to facilitate the piston motion. CFX does not have an explicit two-dimensional solver, so When modeling two dimensional simulations it is recommended that the domain is set to one cell thick and symmetry conditions placed on either side. The modelling advice suggests that the thickness of this cell should be comparable to the size of the smallest cell.

The physics for the simulation were held constant. Homogeneous multiphase, with second-order transient and coupled volume-fraction solution were used in the solver control. The only parameter to vary over the three simulation runs was the time step. This was to ensure that the CFL remained constant. In adherence to recommendations by CFX support, the CFL number was

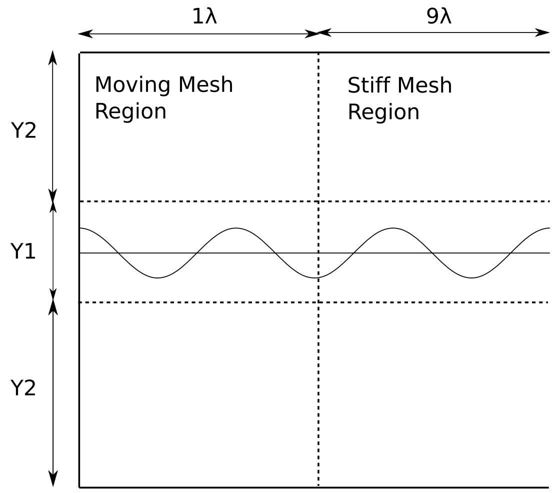


Figure 4: Grid layout corresponding to table 1

Table 2: CFL number

| | Coarse | Medium | Fine |
|---|---|---|---|
| Δ t [s] | 0.04 | 0.02 | 0.01 |
| CFL | 1.56 | 1.56 | 1.56 |

maintained between 1-2.

$$CFL = \frac{\Delta t u}{\Delta x} \tag{49}$$

The paddle motion was ramped up over two seconds, as such, the fully developed wave train should have travelled the length of the flume at the group speed, $c_g$ of $0.78[m/s]$ thus taking no less than $22[s]$. This was one of the criteria examined when looking for the suitability of CFX in handling free surface waves. Isosurface plots with the volume fraction = 0.5 at every 1 second time interval are shown in figure (5). It shows how the waves travel down the flume for the three grids. The vertical dotted line is placed at intervals of $1\lambda$ $(1.56[m])$.

### 4.1 Wave making results in CFX

Upon implementation of the aforementioned settings, the coarse mesh (fig. 5a) showed large damping of the progressive waves in the flume. The wave height decreased considerably and this decrease persisted over time. Also, there seemed to be an unexpected increase in the wave length of the generated waves. A wave of period $T = 1[s]$ was expected and under the water depth conditions, a wave length of $1.56[m]$ was anticipated. As can be seen, (fig. 5a) shows the wave crest getting progressively further apart.

The medium mesh (fig. 5b) doesn't show as severe damping of the free surface elevation as the coarse mesh, but there is still some damping persistant. Again, the waves generated seem to be of a longer wave length than expected. This can be seen looking at the distance the wave crest deviated from the vertical lines. These lines are at one wave length $\lambda = 1.56[m]$ intervals.

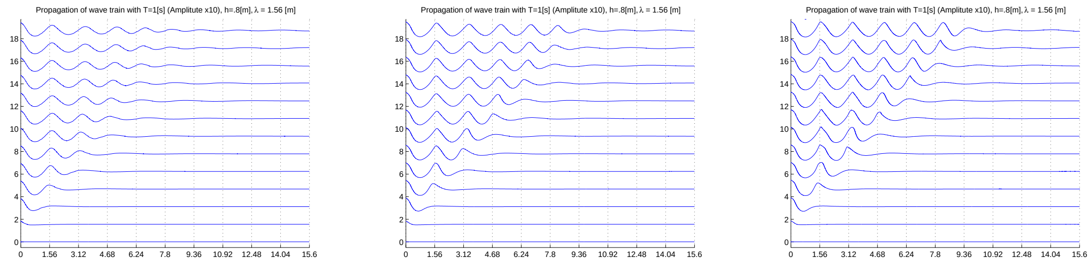

**(a)** Coarse mesh **(b)** Medium mesh **(c)** Fine mesh

**Figure 5:** Wave train propagation over time for coarse, medium and fine mesh

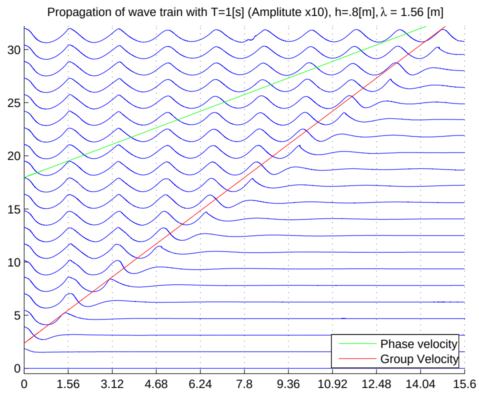


**Figure 6:** Wave propagation through flume with fine mesh over 20s, with time increasing in the Y+ axis direction. Lines showing both group velocity and phase velocity also shown

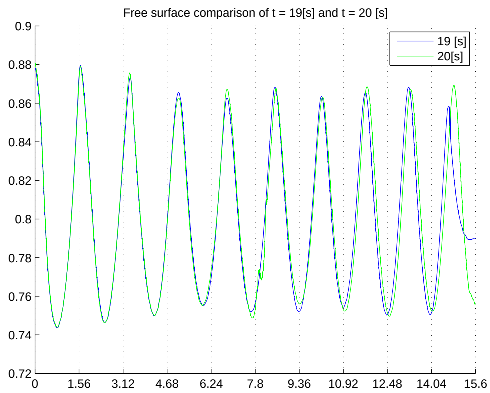


**Figure 7:** Free surface from fine mesh at 19 [s] and 20 [s]. NB the shift in wave peak from time step 19[s] to 20[s] and also the fact that each peak is no aligned with the predicted wave length position

The last refinement was that of the fine mesh (fig. 5c). This shows a little improvement in capturing the free surface elevation when compared to the medium mesh. Overall, the fine mesh is very similar to the medium mesh results. This suggests that CFX is converging, but not on the expected answer. Upon closer analysis of the free surface from the fine mesh, the damping of the waves is more apparent (fig. 7). The expected wave amplitude of $0.08[m]$ does not materialise. There is a steady decline in wave amplitude which plateaus at 4 wavelengths. There seems to be a shift in wavelength also in these simulations. The wave flume expected to have exactly 10 fully developed waves after 20 [s] this was not the case and there were only 9.5 full waves in the flume.

In order to absorb waves, you must first be able to make accurate and precise waves. This did not prove to be the case in ANSYS CFX. There was persistant damping in the flume and an anomaly where there seemed to be a shift in frequencies that resulted in longer wavelengths in the flume.

Current work includes investigation into other commercial CFD codes and feasibility studies are underway.

# 5 Conclusions

In conclusion, this paper has presented the fundamental theory behind the wavemaking process. It has presented the hydrodynamic coefficients of added mass and damping for four different paddle shapes. Two of these novel shaped wavemakers have been discussed how the choice of geometry can effect the wave absorption especially in conjunction with tuning frequency. It has shown the there is potential for improved absorption when the both the geometry and the tuning frequency of a wavemaker/absorber can be adjusted. Results from a solid moving boundary in ANSYS CFX were presented and the CFD simulations do not match the expected results.

**Acknowledgements**

The authors wish to acknowledge funding for this project from the UK Engineering and Physical Sciences Research Council (EPSRC) as part of the Doctoral Training Programme of Phase 2 of SuperGEN MARINE (EP/E040136/1).

Dr Ingram acknowledges the support from Scottish Funding Council of his position within the the Joint Research Institute in Energy with the Heriot-Watt University which is a part of the Edinburgh Research Partnership in Engineering and Mathematics (ERPem).

Comments from A.Price and M.Captieux are greatly appreciated.

## References


[1] T. H. Havelock. Forced surface-waves on water. *Philosophical Magazine*, 3:569–576, October 1929.

[2] F. Biésel and F. Suquet. Les appareils generateurs de houle en laboratorie. *La Houille Blanche*, 6, 1951.

[3] F. Biésel and F. Suquet. Laboratory wave generationg apparatus. *St. Antony Falls Hudraulic Report*, (39), March 1954. Translation from La Houille Blance.

[4] F. Ursell, R.G. Dean, and Y.S. Yu. Forced small amplitude water waves: a comparison of theory and experiment. *Journal of Fluid Mechanics*, 7:33–52, 1960.

[5] R. Hudspeth, J. W. Leonard, and M.-C. Chen. Design curves for hinged wavemakers. In *Proceedings of ASCE, Hydraulics Division*, volume 107, pages 553–574, May 1981.

[6] G. Gilbert, D.M. Thompson, and A.J. Brewer. Design curves for regular and random wave generators. *Journal of Hydraulic Research*, 1970.

[7] J. H. Milgram. Active water-waver absorbers. *Journal of Fluid Mechanics*, 43:845–859, 1970.

[8] S. H. Salter. Absorbing wavemakers and wide tanks. In *Proc. Directional Wave Spectra Applications*, pages 182–202. Berkley, California, 1981.

[9] I. Orlansky. A simple boundary condidtion for unbounded hyperbolic flows. *Journal of Computational Physics*, 21:251–269, 1976.

[10] J. E. Romate. Absorbing boundary conditions for free surface waves. *Journal of Computational Physics*, 99:135–145, 1992.

[11] C. Maisondieu and A. Clement. A realizable force feedback-feedforward control loop for a piston wave absorber. In *Eight international workshop on waver waves adn floating devices*, volume 1, pages 79–82, 1993.

[12] A. Clément and C. Maisondieu. Comparison of time domain control laws for a piston wave absorber. In *Proc. European Wave Energy Symposium*, pages 117–122, 1993.

[13] G. Chatry and A. Clément. Self-adaptive control of a pisoton wave absorber. In *Proc. of 8th Int. Offshore Polar Engineering Conference*, volume 1, pages 127–133, 1998.

[14] J. N. Newman. Analysis of wave generators and absorbers in basins. *Submitted for publication - http://www.wamit.com/publications.htm*, 2008.

[15] J. Spinneken and C. Swan. Wave generation and absorption using force-controlled wave machines. In *Proceedings ISOPE, Osaka*, 2009.

[16] S. Naito. Wave generation and absorption in wave basins: Theory and application. *International Journal of Offshore and Polar Engineers*, 16(2):81–89, 2006.

[17] J. Falnes. *Ocean Waves and Oscillation Systems*. Cambridge University Press, 2002.

[18] A. A. E. Price. *New Persipectives on Wave Energy Converter Control*. PhD thesis, The University of Edinburgh, 2009.